Research paper

The Holocene
2018, Vol. 28(3) 455–463

DOI: 10.1177/0959683617729445
journals.sagepub.com/home/hol
SAGE

Prehistoric heavy metal pollution on the continental shelf off Hainan Island, South China Sea: From natural to anthropogenic impacts around 4.0 kyr BP

Fangjian Xu,[1,2,3] Bangqi Hu,[3,4] Yanguang Dou,[4] Zhaojun Song,[2] Xiting Liu,[5] Shengqiang Yuan,[6] Zhilei Sun,[3,4] Anchun Li[5] and Xuebo Yin[5]

Abstract

Human–environment interactions across historical periods in China have been well reconstructed over the past decade; however, few studies have focused on southern China, particularly Hainan Island. This study investigated two sediment cores (cores X1 and X2) collected from the continental shelf off Hainan Island in the northern South China Sea. Combined with geochemical compositions (Al, Ni, Cu, Zn, Cd, and Pb), Sr-Nd isotopes, grain size, and AMS ^{14}C ages, our results showed that Cd and Cu in core X1 and Cd and Pb in core X2 have been mainly influenced by anthropogenic activities since ~4.0 kyr BP. The enrichment factors showed obvious increases starting at ~4.0 kyr BP and were in good accordance with the appearance of abundant archeological sites on Hainan Island. Significant climatic changes (i.e. decreases in the East Asian summer monsoon and increases in El Niño–Southern Oscillation activities) at ~4.0 kyr BP likely promoted more intense, localized human activities, which in turn enhanced heavy metal accumulation in the continental shelf sediments. These results provide new insights into the history of human activities on Hainan Island and indicate that the geochemical compositions of continental shelf sediments have the potential for broadening our knowledge of the human activities and cultural development in tropical areas.

Keywords

continental shelf, Hainan Island, heavy metals, human activity, sediment, South China Sea

Received 3 January 2017; revised manuscript accepted 11 July 2017

Introduction

Environmental changes are driven by natural forces as well as by human impacts (Dräger et al., 2016; Kalis et al., 2003; Lee et al., 2008; Taylor et al., 2016), and human activities can also have considerable impacts on the natural environment (Kalis et al., 2003; Lee et al., 2008; Maslennikova and Udachin, 2016). Reconstructing historical human development and environmental change is one of the most important tasks in current scientific research. Traditionally, human impacts have been reconstructed via variations in pollen (Broothaerts et al., 2014; Garcés-Pastor et al., 2016), charcoal (Lee et al., 2014), and heavy metals (Guo and Yang, 2016; Lee et al., 2008; Wan et al., 2015). Heavy metals are considered the most toxic pollutants in ecosystems because of their persistence in the environment, bioaccumulation, and high toxicity. Heavy metals can enter the drainage system through runoff and eventually accumulate in the sediments (Fan et al., 2007; Lee et al., 2008; Wan et al., 2015; Xu et al., 2015, 2016a). Previous studies have demonstrated that historical heavy metal accumulation data from sediment cores collected at the coastal/shelf/slope are valuable archives of human activities within the catchment (Kadhum et al., 2016; Lee et al., 2008; Wan et al., 2015).

Because of its vast territory and long history of human civilization, China is a favorable region for studies of historical human–environment interactions. However, these studies have primarily focused on North and Central China (Wu and Liu, 2004, and references therein); historical human–environment interactions in southern China remain less well known (Li et al., 2006;

[1]School of Geosciences, China University of Petroleum, China
[2]Shandong Provincial Key Laboratory of Depositional Mineralization & Sedimentary Minerals, College of Earth Science and Engineering, Shandong University of Science and Technology, China
[3]Laboratory for Marine Mineral Resources, Qingdao National Laboratory for Marine Science and Technology, China
[4]Key Laboratory of Marine Hydrocarbon Resources and Environmental Geology, Ministry of Land and Resources, Qingdao Institute of Marine Geology, China
[5]Institute of Oceanology, Chinese Academy of Sciences, China
[6]Research Institute of Petroleum Exploration and Development, PetroChina, China

Corresponding authors:
Bangqi Hu, Key Laboratory of Marine Hydrocarbon Resources and Environmental Geology, Ministry of Land and Resources, Qingdao Institute of Marine Geology, Qingdao 266071, China.
Email: bangqihu@gmail.com

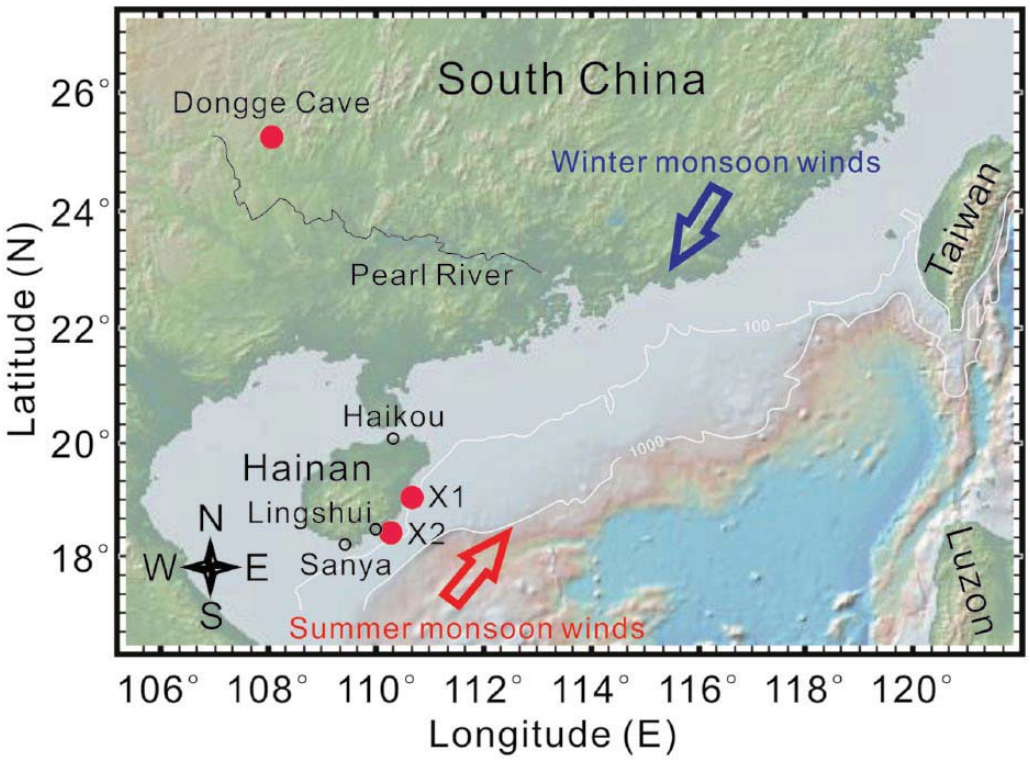

Figure 1. Map of the monsoon winds and locations of cores X1 and X2 (red dots). The monsoon winds are displayed (Webster et al., 1998). The location of Dongge Cave is also displayed (Dykoski et al., 2005). The base map was generated with GeoMapApp (http://www.geomapapp.org).

Wan et al., 2015). Based on palynological research on sediment cores from the Red River Delta, Li et al. (2006) found that human impacts intensified after 3.34 kyr BP. Using sediment cores from the northern continental slope of the South China Sea (SCS), Wan et al. (2015) found that sulfur-related metals (As, Pb, Cu, Mo, and W) and their corresponding enrichment factors (EFs) strongly increased after 1.8 kyr BP. They argued that enhanced human activities have overwhelmed natural climatic erosion control mechanisms within the Red River Basin since then. Until now, little information was available on the historical human–environment interactions at the southernmost tip of China, i.e. Hainan Island.

Hainan Island, with a surface area of 35.4×10^3 km^2, is located in the northern SCS and is the second largest island in China (Figure 1). Recent studies have shown that the sediments in the continental shelf area around Hainan Island contain a wealth of information regarding the paleoenvironmental evolution and anthropogenic activity in this region (Tian et al., 2015; Wu et al., 2007; Xu et al., 2016a, 2016b). However, research in this area has primarily focused on variations in clay minerals (Tian et al., 2015; Wu et al., 2007) and the spatial distributions of heavy metals (Hu et al., 2013; Xu et al., 2016a, 2016b). The earliest cultural relics on Hainan Island were found at the Luobidong Site at Sanya City (Figure 1), which was dated to 10,642 ± 207 yr BP (Yan, 2006). Studies at Neolithic sites have found that the ancient people gradually migrated to the coastal area of Hainan Island after ~6 kyr BP (Qiu, 2015). Information on human–environment interactions in these historical periods, to the best of our knowledge, remains limited in this region. This study presents the results of the analysis of the heavy metals (Ni, Cu, Zn, Cd, and Pb) content in two sediment cores (X1 and X2) from the eastern continental shelf off Hainan Island to (1) determine the historical record (~7.6 kyr) of heavy metal accumulations and then assess the potential impact of anthropogenic activities and (2) obtain information on the historical human–environment interactions in the Hainan region.

Materials and methods

Study area and sampling sites

Hainan Island is characterized by a seasonal and oceanic tropical climate, with annual average temperatures ranging between 22.8°C and 25.8°C and annual rainfall between 961 and 2439 mm yr^{-1} (Zhang et al., 2013). This area is typical of the East Asian monsoon system, with a strong northeasterly monsoon during the winter and a reversal to a southwesterly monsoon during the summer (Liu and Xie, 1999). The water depth along the east coast of Hainan Island decreases sharply from the northwest to the southeast, with isobaths that are parallel to the coastline (Huang et al., 2013).

Sediment cores X1 and X2 were collected from the eastern continental shelf off Hainan Island (Figure 1) using a gravity corer on R/V Shiyan 3 of the South China Sea Institute of Oceanology, Chinese Academy of Sciences, in September 2012. The cores X1 (19°3.23′ N, 110°41.566′ E at a water depth of 52 m) and X2 (18°25.753′ N, 110°17.079′ E at a water depth of 77 m) were 120-cm and 240-cm long, respectively. After collection, they were frozen for preservation until further laboratory analysis and then split, described, photographed, and sampled at the Institute of Oceanology, Chinese Academy of Sciences (IOCAS).

Radiocarbon ages

Mixed benthic foraminifers were analyzed at eight depths for cores X1 and X2 by Beta Analytic (Miami, Florida, US). Raw radiocarbon dates were converted into calibrated calendar ages using CALIB 7.0.2 and by applying the Marine13 program (http://calib.qub.ac.uk/calib; Reimer et al., 2013). Yu et al. (2010) revealed that large fluctuations in the radiocarbon marine reservoir ages and regional marine reservoir corrections occurred in the SCS over the past 7.5 kyr. Therefore, reservoir age correction values of −23 ± 52 years for modern values and 151 ± 85 years for the period 7.5–5.6 kyr BP were adopted based on Yu et al. (2010). All dates were reported in calibrated years before present (with the 'present' representing AD 1950).

Table 1. Certified and measured values of the Al (%) and heavy metal concentrations (mg kg^{-1}) in the standard reference materials (GBW07316, BHVO-2, and BCR-2).

	Element	Al	Ni	Cu	Zn	Cd	Pb
GBW07316	Certified values	7.7 ± 0.3	108 ± 9	231 ± 10	142 ± 22	0.3	22 ± 5
	Measured values	8.2	107	227	141	0.308	21.9
BHVO-2	Certified values	13.5 ± 0.2	119 ± 7	127 ± 7	103 ± 6	NA	NA
	Measured values	14.2	114	142	115	0.345	1.6
BCR-2	Certified values	13.5 ± 0.2	NA	19 ± 2	127 ± 9	NA	11 ± 2
	Measured values	13.8	13	25	138	1.436	10.5

NA: not available.

Grain-size analysis

The samples used for the grain-size analysis were collected at 2-cm intervals, and 59 and 120 samples were analyzed for cores X1 and X2, respectively. All samples were pretreated with excess 30% H_2O_2 and then with 1 mol L^{-1} HCl in a water bath at 60°C for 1 h to remove organic matter and calcium carbonate, respectively. The grain-size samples were dispersed and homogenized using ultrasound before passing through a Cilas 940L Particle Size Analyzer, which accounts for grains in the size range of 0.5 to 2000 μm. The measurement repeatability of the instrument is 0.5%, and the reproducibility is better than 2%.

Sr-Nd isotopes and elemental analysis

Samples used for Sr and Nd isotope analysis were collected at ~20- to ~30-cm intervals, and 4 and 11 samples were analyzed from cores X1 and X2, respectively. Prior to analysis, the <63 μm fraction was wet sieved from the bulk sediments to remove the coarse fraction, dried at 60°C in a clean oven, and ground using an Agate mortar and pestle. All samples were leached sequentially with excess 15% H_2O_2 and then 25% HAc in a water bath at 60°C for 1 h to remove the carbonate and organic fractions (Bayon et al., 2002; Wan et al., 2015). The Sr and Nd isotopic compositions were determined with a multi-collector inductively coupled plasma mass spectrometer (MC-ICP-MS) at the First Institute of Oceanography, State Oceanic Administration, China. The reported $^{87}Sr/^{86}Sr$ and $^{143}Nd/^{144}Nd$ ratios were normalized to the NBS SRM987 standard ($^{87}Sr/^{86}Sr = 0.710250$) and the Shin Etsu JNdi-1 standard ($^{143}Nd/^{144}Nd = 0.512115$) (Tanaka et al., 2000), respectively. Nd isotopic data are expressed as $\varepsilon_{Nd} = [(^{143}Nd/^{144}Nd_{(measured)}/^{143}Nd/^{144}Nd_{(CHUR)}) - 1] \times 10^4$. The CHUR (Chondritic Uniform Reservoir) value is 0.512638 (Jacobsen and Wasserburg, 1980).

Samples of the major element (Al) and heavy metals (Ni, Cu, Zn, Cd, and Pb) were collected at 2-cm and 4-cm intervals for cores X1 (59 samples) and X2 (60 samples), respectively. For elemental analysis, the bulk samples were pretreated with 30% H_2O_2 followed by 1 mol L^{-1} HCl in a water bath at 60°C for 1 h to remove organic matter and calcium carbonate, respectively. The residues were rinsed using deionized water and then heated to dryness at 60°C. All residual samples were ground into powders using an Agate mortar and pestle. After being dissolved with an $HF + HNO_3 + HClO_4$ acid mixture, the concentrations of the major and trace elements were determined using a Thermo iCAP 6300 ICP-AES and Perkin-Elmer ELAN DRC II ICP-MS at IOCAS, respectively. The precision and accuracy were monitored by analyzing selected United States Geological Survey (USGS) and Chinese certified reference materials (BCR-2, BHVO-2, and GBW07316). The differences between the measured and certified values were generally less than 10%, indicating satisfactory recoveries (Table 1).

Enrichment factor

The EF of the metals in the sediments were calculated as follows: $EF = (X/Al)_{sample}/(X/Al)_{background}$, where $(X/Al)_{sample}$ and $(X/Al)_{background}$ represent the ratios of the concentrations of metal X and Al in the samples and background references, respectively. EF values of 0.5–1.5 are typical of element levels that reflect the regional rock composition, whereas an EF > 1.5 indicates non-crustal contributions and/or non-natural weathering processes (e.g. anthropogenic influences) (Zhang and Liu, 2002). The key to the EF calculation is the establishment of geochemical background values. The average crustal abundance data or the average shale values are normally selected as the background values to assess the sediment pollution status; however, using local background values from deep sediment layers not affected by pollution (Wan et al., 2015) might be more appropriate. Previous studies have found that the first phase of rice cultivation in the Pearl River Basin occurred approximately 4.8–4.3 kyr BP (Zhang et al., 2007; Zong et al., 2013). Earlier studies speculated that the primitive agriculture of Hainan Island originated approximately 3.0 kyr BP (Hainan Provincial Office of Local History, 1997; Yan, 2006). From 5.0 kyr BP onward, the Southeast Asian island region has witnessed a continuous expansion of agricultural populations (Bellwood, 1987). Approximately 130 Neolithic cultural sites have been discovered on Hainan Island, and most of those appeared after 5.0 kyr BP (Yan et al., 2013). Therefore, it is reasonable to select the mean values of the sediment samples from cores X1 and X2 deposited before 5.0 kyr BP as their natural background values.

Sequential regime shift detection

The EF data sets were analyzed for regime shifts using Sequential Regime Shift Detector (version 3.4) with the red-noise estimation and pre-whitening options (Rodionov, 2004). The program uses a *t* tests sequential algorithm to determine whether the next value is significantly different from the previous regime. The determination of the regimes is strongly influenced by the choice of the cutoff length *l* and the significance level *p* of the *t* tests (see details in Rodionov, 2004). We used $l = 10$ and $p = 0.1$ for the analysis of our time series.

Results

Core lithology and age model

Core X1 mainly consists of silty sand and sandy silt that are partially mixed with shell fragments. Based on a visual inspection of the color, texture, and structure, core X1 can be divided into two depositional units: Unit I represents depths from 120 to 46 cm and consists of silty sand and sandy silt with shell fragments, and Unit II represents depths from 46 to 0 cm and primarily consists of sandy silt partially mixed with shell fragments. The 31- to 0-cm section gradually turns light brown, with uniform lithology.

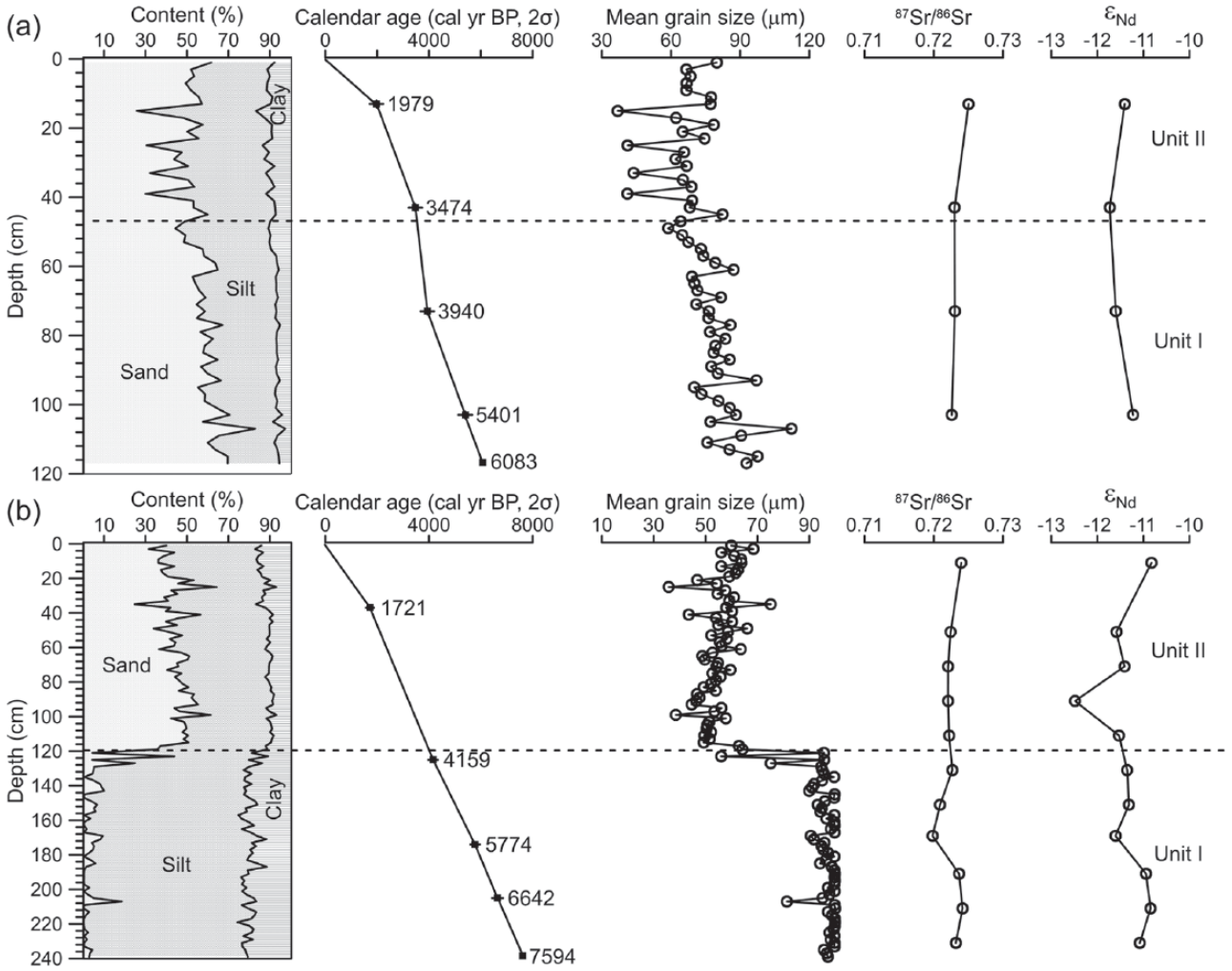

Figure 2. Sand, silt, and clay content, calibrated ages, mean grain size, and Sr and Nd isotope ratios in the sediments of cores (a) X1 and (b) X2. The ages of the base are estimated ages based on extrapolation.

Core X2 can be divided into two depositional units: Unit I represents depths from 240 to 120 cm and consists of blue-gray mud interspersed with occasional sandy lenses with shell fragments, and Unit II represents depths from 120 to 0 cm in depth and primarily consists of blue-gray silty sand and sandy silt partially mixed with shell fragments. The 20- to 0-cm section gradually turns light brown, with uniform lithology.

The downcore variations in the mean grain sizes for cores X1 and X2 are shown in Figure 2. Upper Unit II of core X1 contains more silt and clay but less sand, thereby resulting in lower mean grain sizes in this unit (Figure 2a). However, upper Unit II of core X2 contains more sand but less silt and clay, thereby resulting in higher mean grain sizes in this unit (Figure 2b).

The age models of each sampling interval were established via linear interpolations between each adjacent pair of calendar ages. The basal ages of cores X1 and X2 are ~6.1 and ~7.6 kyr BP, respectively, as estimated by an extrapolation of the linear interpolation between their two oldest dates (Table 2 and Figure 2). The average sedimentation rates are 19.7 and 31.6 cm kyr^{-1} for cores X1 and X2, respectively.

Sr-Nd isotope compositions and elemental concentrations

Downcore variations in the Sr-Nd isotopic ratios are shown in Figure 2. The $^{87}Sr/^{86}Sr$ ratios in core X1 vary between 0.72260 and 0.72503, and the $^{143}Nd/^{144}Nd$ ratios range from 0.512037 to 0.512063 (−11.7 to −11.2 for ε_{Nd}). The $^{87}Sr/^{86}Sr$ ratios in core X2 vary between 0.71983 and 0.72416, and the $^{143}Nd/^{144}Nd$ ratios range from 0.511998 to 0.512083 (−12.5 to −10.8 for ε_{Nd}). Overall, $^{87}Sr/^{86}Sr$ and ε_{Nd} in the sediments of cores X1 and X2 were relatively stable, with occasional extreme values at certain depths.

The metal concentrations in core X1 were 6.9–11.0% for Al, 12.5–25.0 mg kg^{-1} for Ni, 8.7–18.7 mg kg^{-1} for Cu, 39.4–70.2 mg kg^{-1} for Zn, 0.07–0.21 mg kg^{-1} for Cd, and 9.9–18.8 mg kg^{-1} for Pb. The metal concentrations in core X2 were 8.8–17.5% for Al, 14.1–35.2 mg kg^{-1} for Ni, 11.9–24.8 mg kg^{-1} for Cu, 47.5–103.4 mg kg^{-1} for Zn, 0.20–0.42 mg kg^{-1} for Cd, and 11.6–20.2 mg kg^{-1} for Pb. The concentrations of Al, Ni, Cu, and Zn display remarkable changes at approximately 3.6 and 4.0 kyr BP in cores X1 and X2, respectively. They are low in core X1 and high in core X2 in Unit I, and the opposite results were found for Unit II. As noted above, the changes in lithology differ significantly between cores X1 and X2 (Figure 2). These concentrations were mainly controlled by the different lithologies, indicating the 'grain size effect on element concentrations' (Yang et al., 2002; Zhang et al., 2002). The concentrations of Cd increased upward in cores X1 and X2, whereas the concentrations of Cu and Pb increased upward in cores X1 and X2, respectively (Figure 3).

Discussion

Influence factors on heavy metals and pollution assessments

The Sr-Nd isotopic compositions of the sediments are credible proxies for tracing the provenance, transport, and deposition

Table 2. AMS ^{14}C dating of cores X1 and X2.

Core	Laboratory number	Depth (cm)	$^{13}C/^{12}C$ (‰)	^{14}C age (yr BP)	Calendar age (cal. yr BP, 2σ)
X1	427661	12–14	1.1	2330 ± 30	1979 (1827–2130)
	425274	42–44	0.4	3550 ± 30	3474 (3331–3616)
	425275	72–74	0.6	3920 ± 30	3940 (3761–4118)
	380799	102–104	−1.8	5000 ± 30	5401 (5259–5542)
X2	350316	36–38	−0.2	2120 ± 30	1721 (1569–1872)
	346831	124–126	−0.6	4080 ± 30	4159 (3970–4348)
	380798	172–176	−0.4	5560 ± 30	5774 (5585–5962)
	346832	204–206	−1.0	6350 ± 30	6642 (6423–6860)

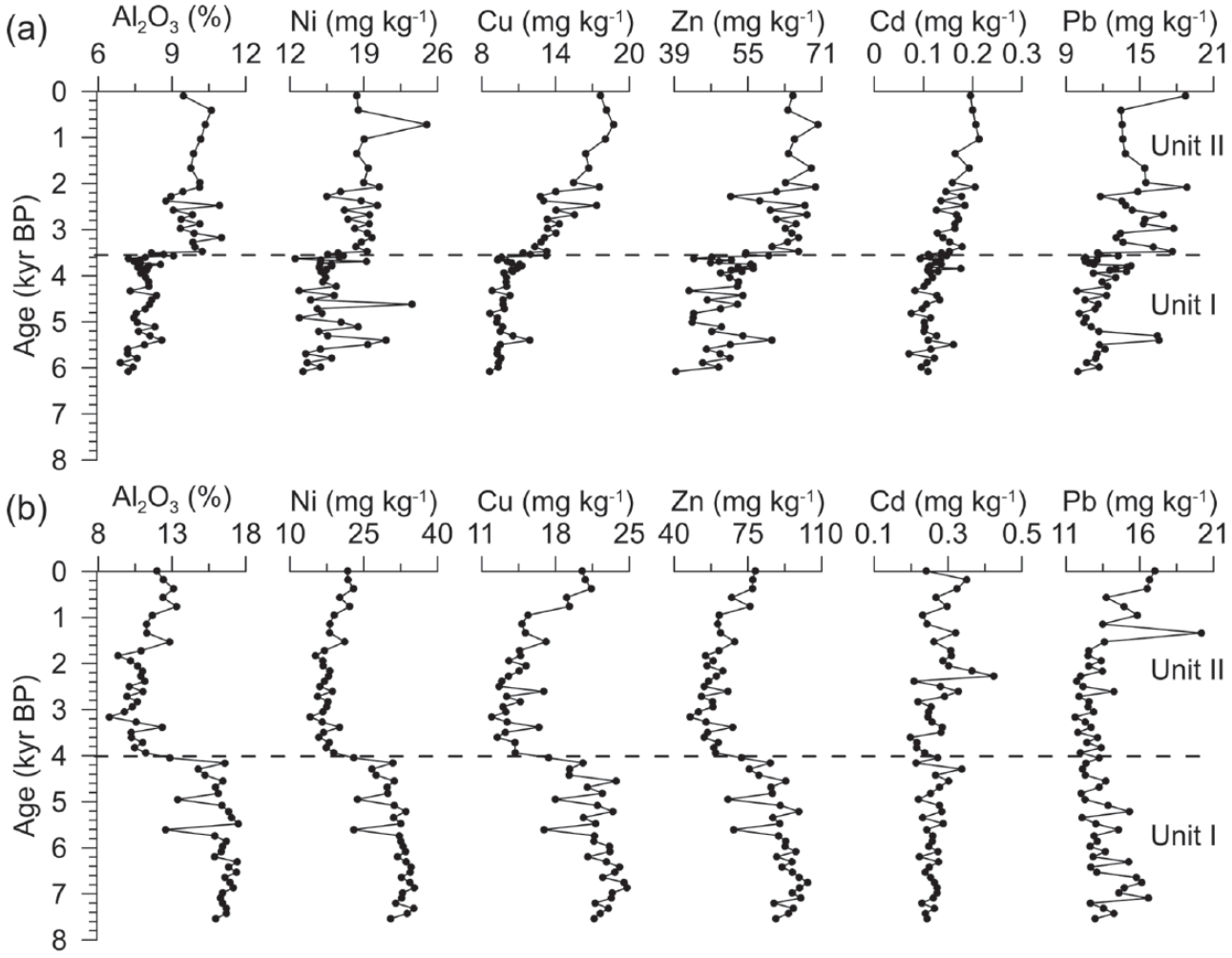

Figure 3. Downcore variations in the geochemical composition of sediment cores (a) X1 and (b) X2.

of various sediments. Overall, $^{87}Sr/^{86}Sr$ and ε_{Nd} in the sediments of cores X1 and X2 indicate that the sediment provenances were relatively stable (Figure 2). Based on the analysis of the mineral assemblages and their distributions in sediment samples, our study area falls into the 'Hainan Island mineral province' (Chen, 2008; Chen et al., 1986). This conclusion has been previously supported by other studies based on the magnetic properties (Tian et al., 2013), clay mineralogy (Hu et al., 2014), and the geochemical record (Yan et al., 2016) of the neighboring region. Thus, we infer that the sediments of cores X1 and X2 were primarily derived from Hainan Island, and no major change in sediment source occurred during the studied periods. In addition, organic matter and fine-grained sediments are important factors controlling the concentrations of heavy metals in bulk sediments (Fan et al., 2007; Hu et al., 2013; Wan et al., 2015; Wang et al., 1997). In this study, the sediment samples have been pretreated with 30% H_2O_2; thus, the measured heavy metal concentrations were not influenced by organic matter. In contrast, most metals were negatively correlated with mean grain size (Table 3), suggesting that heavy metal concentrations in core X1 and X2 were influenced by grain size to a certain extent. A normalization process compensating for the natural variability of metals is a prerequisite for detecting and quantifying the anthropogenic metal contribution.

The EF is widely used to eliminate the influence of grain size on elemental concentrations and to discriminate between natural and anthropogenic sources (Kadhum et al., 2016; Wan et al., 2015). Most of the EF values of the heavy metals (Ni, Cu, Zn, Cd, and Pb) in core X1 vary between 0.6 and 1.5 (Figure 4), implying

Table 3. Pearson's correlation matrix for mean grain size and heavy metal concentrations (Ni, Cu, Zn, Cd, and Pb).

	Ni	Cu	Zn	Cd	Pb
Mean grain size (core X1)	−0.278[a]	−0.497[b]	−0.555[b]	−0.438[b]	−0.453[b]
Mean grain size (core X2)	−0.917[b]	−0.788[b]	−0.869[b]	0.190	−0.037

[a]Correlation is significant at the 0.05 level (two-tailed).
[b]Correlation is significant at the 0.01 level (two-tailed).

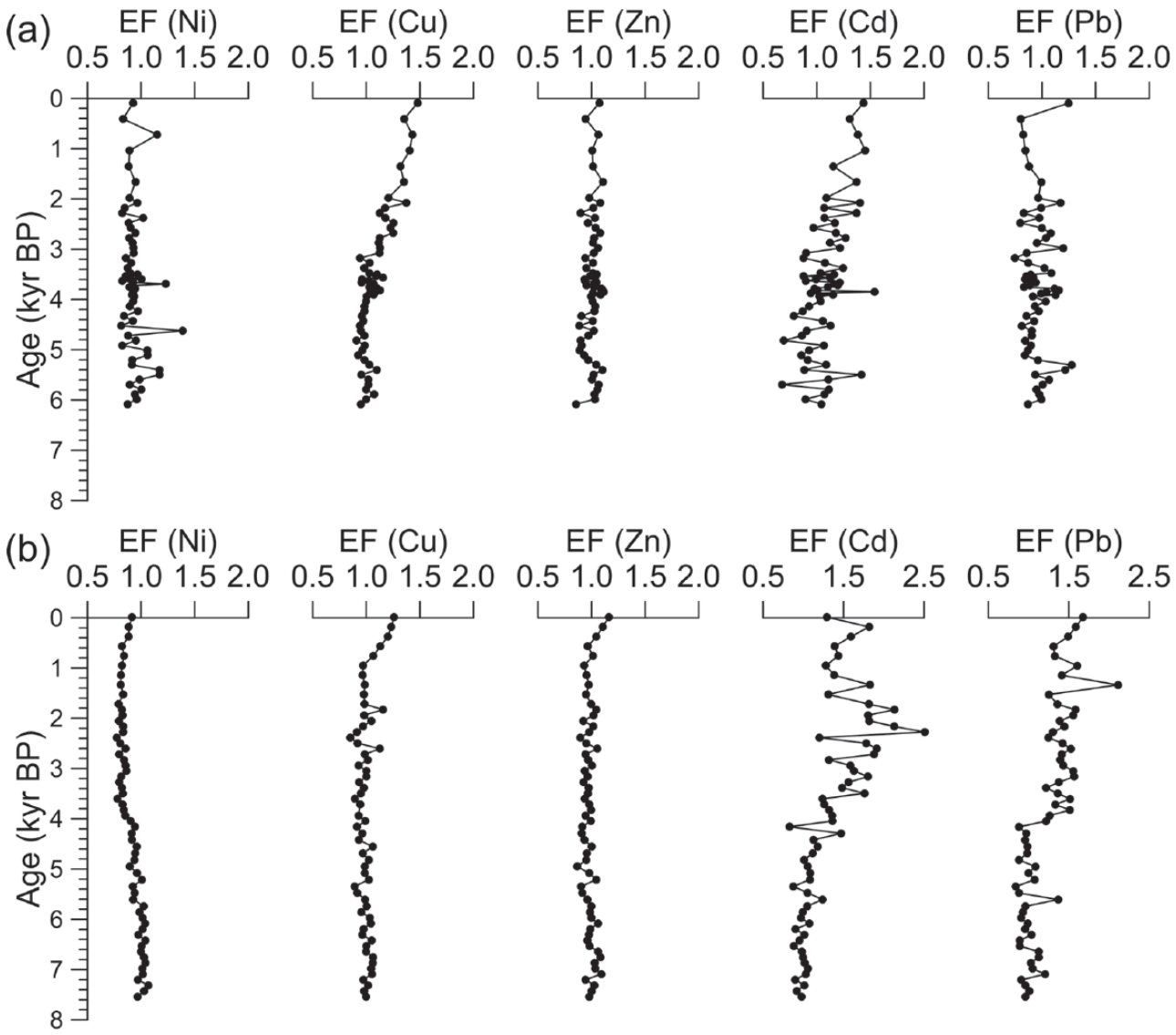

Figure 4. Enrichment factor (EF) for heavy metals (Ni, Cu, Zn, Cd, and Pb) in cores (a) X1 and (b) X2.

that these metals are mainly derived from natural weathering processes. However, the EF values of Cd and Cu displayed stepped increasing trends since ~4.0 kyr BP, as confirmed by the results of regime shift detection (Figures 4 and 5a). The EF values of Ni, Cu, and Zn of core X2 generally varied approximately 1.0, whereas the EF values of Cd and Pb varied approximately 1.0 before ~4.0 kyr BP but increased significantly since then (averaged 1.6 and 1.4, respectively) (Figures 4 and 5b). Although the lithology differs between cores X1 and X2, the EF values of Cd for both cores (as well as Cu for core X1 and Pb for core X2) display synchronous regime shifts at ~4.0 kyr BP (Figures 5a and 5b). This finding suggests that anthropogenic activities (e.g. mining, smelting, deforestation, and intensive agriculture) on Hainan Island have likely disturbed the natural weathering processes since then.

Human activity in response to paleoclimatic change at 4 kyr BP

Disentangling the effects of climatic change and anthropogenic activities on the environment has received much attention. Previous studies indicated that human activities varied significantly in various regions (Cullen et al., 2000; DeMenocal, 2001; Zhang et al., 2008). Climatic changes that occurred at approximately 4.0 kyr BP, which has been termed the '4.0 kyr event', were particularly devastating, and scholars have argued that this event could have played a role in the collapse of the ancient civilizations in Indus, Egypt, and Mesopotamia (Cullen et al., 2000; DeMenocal, 2001; Innes et al., 2014; Staubwasser et al., 2003). By contrast, the 4.0 kyr event may have had positive effects in the coastal areas of Peru, where severe environmental changes may have promoted agricultural resources over seafood (Kerr, 1998). The 4.0

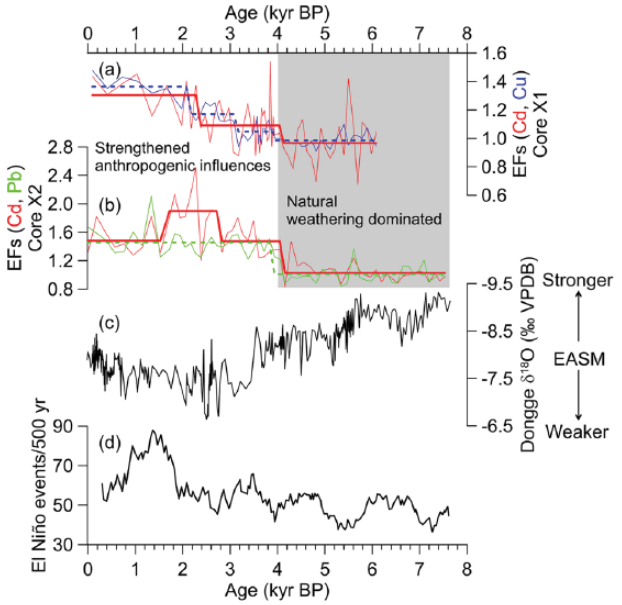

Figure 5. Comparisons of the enrichment factors (EFs) for the heavy metals in cores (a) X1 and (b) X2, (c) the stalagmite $\delta^{18}O$ values from Dongge Cave in southern China (Dykoski et al., 2005), and (d) the modeled El Niño frequency indicating the increase in El Niño events in the tropics (Clement et al., 2000). Regime shifts in the EF values of the metals indicated with colored lines (red solid: Cd, blue dashed: Cu, green dashed: Pb). See Figure 1 for the locations of the cores and the cave.

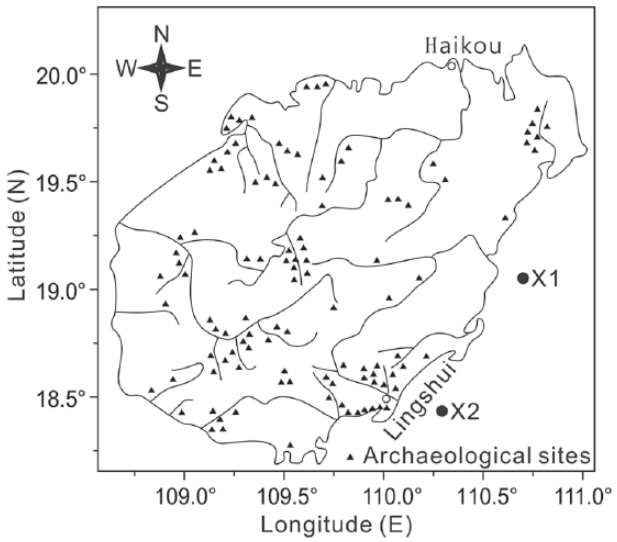

Figure 6. Map of the spatial distribution of archeological sites on Hainan Island. Modified from Yan (2006).

kyr event also facilitated the emergence of Chinese civilization because of increases in the availability of more environmentally circumscribed agricultural lands (Wu and Liu, 2004). Studies of the distribution of prehistoric cultural sites in Zhejiang Province, South China, also showed that the expansion and contraction of prehistoric cultures are positively correlated with climatic change (Wu et al., 2012). In this study area, the archeological sites Shigong and Yinian located in Lingshui County, eastern Hainan, were found and dated to approximately 4.2 and 3.6 kyr BP, respectively (Qiu, 2015; Figure 6). After ~4.0 kyr BP, human impacts were clearly identified in our heavy metal records and detected regime shifts (Figures 5a and 5b). The temporal consistency of the date of the archeological sites and heavy metal variations further suggest that the elevated heavy metal accumulations in the sediment records were primarily caused by human activities in the eastern portion of Hainan Island.

Hainan Island is dominated by the East Asian monsoon system (Liu and Xie, 1999). The intensity of the East Asian summer monsoon (EASM) decreased sharply at approximately 3.6 kyr BP (Dykoski et al., 2005; Figure 5c), and this dramatic event was reflected in changes in the marine sediment records from the SCS (Wang et al., 1999). Analysis of corals in the SCS also showed a major weakening of the monsoon system during the same period (Sun et al., 2005). Changes in the hydrological properties of Hainan Island are also related to El Niño–Southern Oscillation (ENSO) (Su et al., 2013; Zhang et al., 2013). During El Niño events, high SST asymmetry occur in the equatorial Pacific Ocean with a weakened Pacific Walker circulation shifting eastward away from the western Pacific warm pool. These changes result in less rainfall in Southeast Asia (including the SCS) than that during normal conditions (Wu et al., 2003). Modeling studies by Clement et al. (2000) argued that ENSO activities increased during the late Holocene (Figure 5d), and these data were broadly consistent with the ENSO frequency reconstructions based on data from Laguna Pallcacocha, Ecuador (Moy et al., 2002), and from Galápagos lake sediment in the eastern tropical Pacific (Conroy et al., 2008). Thus, both the decreased monsoon intensity and increased ENSO activity since ~4 kyr likely result in less precipitation on Hainan Island.

Furthermore, summer coastal upwelling along eastern Hainan Island has significant impacts on the nearshore ecosystem and fishery because it supplies nutrient-rich deep water to the surface and supports high levels of biological productivity (Su et al., 2013). A 121-year monthly coral Sr/Ca record at Boao (Sanya City) reveals prominent multi-decadal variability in upwelling driven by the Asian summer monsoon, with weak summer coastal upwelling caused by decreased monsoon intensity, and vice versa (Liu et al., 2013). The decreased summer monsoon and increased ENSO activities since ~4.0 kyr BP have caused the summer coastal upwelling along eastern Hainan Island to sharply weaken, which likely reduces summer primary production as well as the seafood catch (Hu et al., unpublished data). The economy (especially the marine economy) of southeastern coastal Zhejiang (nearby Zhoushan upwelling) also experienced considerable setbacks at approximately 4.0 kyr BP because of increased ENSO activity (Wu et al., 2012).

As shown in Figure 5, the elevated EF values of metals are consistent with decreased summer monsoon intensities and increased ENSO activities within the range of age error. This finding suggests that the proportion of agriculture in the coastal areas of Hainan increased significantly and that agriculture became an important production activity in response to the colder and more arid climate since approximately 4.0 kyr BP (Qiu, 2015). Human impacts may have increased because of agricultural developments, deforestation, and metal utilization (Broothaerts et al., 2014; Dodson et al., 2009; Lee et al., 2008; Wan et al., 2015), which has led to elevated heavy metals in the soil. We thus attribute these elevated heavy metal accumulations to the higher demand for natural resources and more intense, localized human activities, which in turn were influenced by climatic change (i.e. decreased EASM and increased ENSO activities) as discussed above.

Conclusion

Cores X1 and X2 were collected from the continental shelf off Hainan Island in the SCS and used to investigate the historical human–environment interactions in the Hainan region. Based on the EF values, the heavy metals Cd and Cu in core X1 and Cd and Pb in core X2 were influenced by anthropogenic activities, indicating that these metals could be used as indicators of human

activities near the Hainan region. The EF values of these metals showed important increases beginning at ~4.0 kyr BP in both cores. This finding is consistent with the abundant archeological sites on Hainan Island that date to approximately 4.0 kyr BP. Enhanced human activities in the Hainan region are synchronous with decreases in the EASM and increases in ENSO activities. Therefore, the elevated EF values of metals in cores X1 and X2 are attributable to more intense, localized human activities, which were influenced by climatic change.

Acknowledgements

The authors would like to thank the editors, Fabienne Marret and Gill Oliver, and the anonymous reviewers for their constructive reviews of our earlier version of this paper and the crews of the South China Sea Open Cruise by R/V Shiyan 3, South China Sea Institute of Oceanology, Chinese Academy of Sciences.

Funding

This study was supported by the funding provided by the National Natural Science Foundation of China (41576058, 41106040, and 41606062), the National Key Basic Research Program of China (2013CB429703), the Science and Technology Basic Research Program in Resource Survey (2017FY201407-1), and the Open Fund of Shandong Provincial Key Laboratory of Depositional Mineralization & Sedimentary Minerals, Shandong University of Science and Technology (DMSM2017076).

References

Bayon G, German CR, Boella RM et al. (2002) An improved method for extracting marine sediment fractions and its application to Sr and Nd isotopic analysis. *Chemical Geology* 187(3–4): 179–199.

Bellwood P (1987) The prehistory of Island Southeast Asia: A multidisciplinary review of recent research. *Journal of World Prehistory* 1(2): 171–224.

Broothaerts N, Verstraeten G and Kasse C (2014) Reconstruction and semi-quantification of human impact in the Dijle catchment, central Belgium: A palynological and statistical approach. *Quaternary Science Reviews* 102: 96–110.

Chen LR (2008) *Sedimentary Mineralogy of the China Sea*. Beijing: China Ocean Press, p. 263 (in Chinese).

Chen LR, Xu WQ, Shen SX et al. (1986) Mineral assemblages and their distribution pattern in the sediments from the north continental shelf of the South China Sea and the Beibu Gulf. *Marine Sciences* 10(3): 6–10 (in Chinese with English abstract).

Clement AC, Seager R and Cane MA (2000) Suppression of El Niño during the Mid-Holocene by changes in the Earth's orbit. *Paleoceanography* 15(6): 731–737.

Conroy JL, Overpeck JT, Cole JE et al. (2008) Holocene changes in eastern tropical Pacific climate inferred from a Galápagos lake sediment record. *Quaternary Science Reviews* 27(11–12): 1166–1180.

Cullen HM, DeMenocal PB, Hemming S et al. (2000) Climate change and the collapse of the Akkadian empire: Evidence from the deep sea. *Geology* 28(4): 379–382.

DeMenocal PB (2001) Cultural responses to climate change during the late Holocene. *Science* 292(5517): 667–673.

Dodson J, Li X, Ji M et al. (2009) Early bronze in two Holocene archaeological sites in Gansu, NW China. *Quaternary Research* 72(3): 309–314.

Dräger N, Theuerkauf M, Szeroczyńska K et al. (2016) Varve microfacies and varve preservation record of climate change and human impact for the last 6000 years at Lake Tiefer See (NE Germany). *The Holocene* 27(3): 450–464.

Dykoski CA, Edwards RL, Cheng H et al. (2005) A high-resolution, absolute-dated Holocene and deglacial Asian monsoon record from Dongge Cave, China. *Earth and Planetary Science Letters* 233(1–2): 71–86.

Fan Q, He J, Xue H et al. (2007) Competitive adsorption, release and speciation of heavy metals in the Yellow River sediments, China. *Environmental Geology* 53(2): 239–251.

Garcés-Pastor S, Cañellas-Boltà N, Clavaguera A et al. (2016) Vegetation shifts, human impact and peat bog development in Bassa Nera pond (Central Pyrenees) during the last millennium. *The Holocene* 27(4): 553–565.

Guo Y and Yang S (2016) Heavy metal enrichments in the Changjiang (Yangtze River) catchment and on the inner shelf of the East China Sea over the last 150 years. *Science of the Total Environment* 543(Pt A): 105–115.

Hainan Provincial Office of Local History (1997) *Hainan Provincial Local-Records Compilation, Agriculture Section*. Haikou: Nanhai Publishing Company, pp. 1–485 (in Chinese).

Hu B, Cui R, Li J et al. (2013) Occurrence and distribution of heavy metals in surface sediments of the Changhua River Estuary and adjacent shelf (Hainan Island). *Marine Pollution Bulletin* 76(1–2): 400–405.

Hu B, Li J, Cui R et al. (2014) Clay mineralogy of the riverine sediments of Hainan Island, South China Sea: Implications for weathering and provenance. *Journal of Asian Earth Sciences* 96: 84–92.

Huang D, Du J, Deng B et al. (2013) Distribution patterns of particle-reactive radionuclides in sediments off eastern Hainan Island, China: Implications for source and transport pathways. *Continental Shelf Research* 57: 10–17.

Innes JB, Zong Y, Wang Z et al. (2014) Climatic and palaeoecological changes during the mid- to Late Holocene transition in eastern China: High-resolution pollen and non-pollen palynomorph analysis at Pingwang, Yangtze coastal lowlands. *Quaternary Science Reviews* 99: 164–175.

Jacobsen SB and Wasserburg GJ (1980) Sm-Nd isotopic evolution of chondrites. *Earth and Planetary Science Letters* 50(1): 139–155.

Kadhum SA, Ishak MY and Zulkifli SZ (2016) Evaluation and assessment of baseline metal contamination in surface sediments from the Bernam River, Malaysia. *Environmental Science and Pollution Research* 23(7): 6312–6321.

Kalis AJ, Merkt J and Wunderlich J (2003) Environmental changes during the Holocene climatic optimum in central Europe – Human impact and natural causes. *Quaternary Science Reviews* 22(1): 33–79.

Kerr RA (1998) Sea-floor dust shows drought felled Akkadian Empire. *Science* 279(5349): 325–326.

Lee CSL, Qi SH, Zhang G et al (2008) Seven thousand years of records on the mining and utilization of metals from lake sediments in central China. *Environmental Science & Technology* 42(13): 4732–4738.

Lee C-Y, Chang C-L, Liew P-M et al. (2014) Climate change, vegetation history, and agricultural activity of Lake Li-yu Tan, central Taiwan, during the last 2.6 ka BP. *Quaternary International* 325: 105–110.

Li Z, Saito Y, Matsumoto E et al. (2006) Climate change and human impact on the Song Hong (Red River) Delta, Vietnam, during the Holocene. *Quaternary International* 144(1): 4–28.

Liu WT and Xie X (1999) Spacebased observations of the seasonal changes of south Asian monsoons and oceanic responses. *Geophysical Research Letters* 26(10): 1473–1476.

Liu Y, Peng Z, Shen C-C et al. (2013) Recent 121-year variability of western boundary upwelling in the northern South China Sea. *Geophysical Research Letters* 40(12): 3180–3183.

Maslennikova AV and Udachin VN (2016) Lakes ecosystem response to Holocene climate changes and human impact in the Southern Urals: Diatom and geochemical proxies. *The Holocene* 27(6): 847–859.

Moy CM, Seltzer GO, Rodbell DT et al. (2002) Variability of El Niño/Southern Oscillation activity at millennial timescales during the Holocene epoch. *Nature* 420(6912): 162–165.

Qiu G (2015) The marine cultural characteristic of the prehistoric sites of Hainan Island. *The Journal of South China Sea Studies* 1(3): 100–103 (in Chinese with English abstract).

Reimer PJ, Bard E, Bayliss A et al. (2013) IntCal13 and Marine13 radiocarbon age calibration curves 0–50,000 years cal BP. *Radiocarbon* 55(4): 1869–1887.

Rodionov SN (2004) A sequential algorithm for testing climate regime shifts. *Geophysical Research Letters* 31(9): L09204.

Staubwasser M, Sirocko F, Grootes PM et al. (2003) Climate change at the 4.2 ka BP termination of the Indus Valley civilisation and Holocene south Asia monsoon variability. *Geophysical Research Letters* 30(8): 1425.

Su J, Xu M, Pohlmann T et al. (2013) A western boundary upwelling system response to recent climate variation (1960–2006). *Continental Shelf Research* 57(1): 3–9.

Sun D, Gagan MK, Cheng H et al. (2005) Seasonal and interannual variability of the Mid-Holocene East Asian monsoon in coral δ18O records from the South China Sea. *Earth and Planetary Science Letters* 237(1–2): 69–84.

Tanaka T, Togashi S, Kamioka H et al. (2000) JNdi-1: A neodymium isotopic reference in consistency with LaJolla neodymium. *Chemical Geology* 168(3–4): 279–281.

Taylor KJ, Stolze S, Beilman DW et al. (2016) Response of chironomids to Neolithic land-use change in north-west Ireland. *The Holocene* 27(6): 879–889.

Tian C, Ouyang T, Zhu Z et al. (2013) Spatial distribution of magnetic susceptibility and its provenance implication of surface sediments in the sea areas around the Hainan Island. *Tropical Geography* 33(6): 666–673 (in Chinese with English abstract).

Tian X, Xu F, Wu S et al. (2015) Clay mineral characteristics and provenance of continental shelf sediments in eastern Hainan Island since middle Holocene. *Earth Science-Journal of China University of Geosciences* 40(9): 1497–1504 (in Chinese with English abstract).

Wan S, Toucanne S, Clift PD et al. (2015) Human impact overwhelms long-term climate control of weathering and erosion in southwest China. *Geology* 43(5): 439–442.

Wang F, Chen J and Forsling W (1997) Modeling sorption of trace metals on natural sediments by surface complexation model. *Environmental Science & Technology* 31(2): 448–453.

Wang L, Sarnthein M, Erlenkeuser H et al. (1999) Holocene variations in Asian monsoon moisture: A bidecadal sediment record from the South China Sea. *Geophysical Research Letters* 26(18): 2889–2892.

Webster PJ, Magana VO, Palmer TN et al. (1998) Monsoons: Processes, predictability, and the prospects for prediction. *Journal of Geophysical Research* 103(C7): 14451–14510.

Wu L, Zhu C, Zheng C et al. (2012) Response of prehistoric culture to climatic environmental changes since Holocene in Zhejiang, East China. *Acta Geographica Sinica* 67(7): 903–916 (in Chinese with English abstract).

Wu M, Li SR, Chu FY et al. (2007) The assemblage and environmental significance of clay minerals in the surficial sediments around Haiman Island. *Journal of Mineralogy and Petrology* 27(2): 101–107 (in Chinese with English abstract).

Wu R, Hu ZZ and Kirtman BP (2003) Evolution of ENSO-related rainfall anomalies in East Asia. *Journal of Climate* 16(22): 3742–3758.

Wu W and Liu T (2004) Possible role of the 'Holocene Event 3' on the collapse of Neolithic Cultures around the Central Plain of China. *Quaternary International* 117(1): 153–166.

Xu F, Qiu L, Cao Y et al. (2016a) Trace metals in the surface sediments of the intertidal Jiaozhou Bay, China: Sources and contamination assessment. *Marine Pollution Bulletin* 104(1–2): 371–378.

Xu F, Tian X, Yin F et al. (2016b) Heavy metals in the surface sediments of the northern portion of the South China Sea shelf: Distribution, contamination, and sources. *Environmental Science and Pollution Research* 23(9): 8940–8950.

Xu F, Tian X, Yin X et al. (2015) Trace metals in the surface sediments of the eastern continental shelf of Hainan Island: Sources and contamination. *Marine Pollution Bulletin* 99(1–2): 276–283.

Yan GL, Liu FS and Chang RY (2013) *Hainan History & Culture No.3*. Beijing: Social Sciences Academic Press, p. 39 (in Chinese).

Yan H, Tian X, Xu F et al. (2016) Sediment provenance of offshore mud area of the eastern Hainan Island in South China Sea since the Mid-Holocene. *Acta Oceanologica Sinica* 38(7): 97–106 (in Chinese with English abstract).

Yan JA (2006) Paleontology and ecologic environmental evolution of the Quaternary in Hainan Island. *Journal of Palaeogeography* 8(1): 103–115 (in Chinese with English abstract).

Yang SY, Li CX, Jung HS et al. (2002) Discrimination of geochemical compositions between the Changjiang and the Huanghe sediments and its application for the identification of sediment source in the Jiangsu coastal plain, China. *Marine Geology* 186(3–4): 229–241.

Yu K, Hua Q, Zhao J et al (2010) Holocene marine 14C reservoir age variability: Evidence from 230th-dated corals in the South China Sea. *Paleoceanography* 25: PA3205.

Zhang C, Wang L, Li G et al. (2002) Grain size effect on multielement concentrations in sediments from the intertidal flats of Bohai Bay, China. *Applied Geochemistry* 17(1): 59–68.

Zhang J and Liu CL (2002) Riverine composition and estuarine geochemistry of particulate metals in China – Weathering features, anthropogenic impact and chemical fluxes. *Estuarine, Coastal and Shelf Science* 54(6): 1051–1070.

Zhang J, Wang DR, Jennerjahn T et al. (2013) Land–sea interactions at the east coast of Hainan Island, South China Sea: A synthesis. *Continental Shelf Research* 57: 132–142.

Zhang P, Cheng H, Edwards RL et al. (2008) A test of climate, sun, and culture relationships from an 1810-year Chinese cave record. *Science* 322(5903): 940–942.

Zhang W, Xiang A, Qu L et al. (2007) Research on the husks of ancient rice in the Shixia Ruins. *Journal of South China Agricultural University* 28(2): 20–23 (in Chinese with English abstract).

Zong Y, Zheng Z, Huang K et al. (2013) Changes in sea level, water salinity and wetland habitat linked to the late agricultural development in the Pearl River delta plain of China. *Quaternary Science Reviews* 70: 145–157.